Electroreceptor neuron dynamics shape information transmission

Maurice J Chacron[1], Leonard Maler[2] & Joseph Bastian[1]

The gymnotiform weakly electric fish *Apteronotus leptorhynchus* can capture prey using electrosensory cues that are dominated by low temporal frequencies. However, conventional tuning curves predict poor electroreceptor afferent responses to low-frequency stimuli. We compared conventional tuning curves with information tuning curves and found that the latter predicted substantially improved responses to these behaviorally relevant stimuli. Analysis of receptor afferent baseline activity showed that negative correlations reduced low-frequency noise levels, thereby increasing information transmission. Multiunit recordings from receptor afferents showed that this increased information transmission could persist at the population level. Finally, we verified that this increased low-frequency information is preserved in the spike trains of central neurons that receive receptor afferent input. Our results demonstrate that conventional tuning curves can be misleading when certain noise reduction strategies are used by the nervous system.

The identification of behaviorally relevant neural codes is a principal goal of studies of sensory processing systems[1,2]. Progress toward this goal requires that neural codes be understood from the organism's point of view, or in a more limited sense, from the postsynaptic cell's point of view. Experimental studies verifying that postsynaptic cells actually decode information encoded by a particular presynaptic activity pattern are needed in order to further our understanding of these codes[3]. Various methodologies have been used to specify which aspects of a stimulus are represented in a single neuron's pattern of activity or spike train. These methods range from simple measures of changes in firing frequency[4] or spike count[5] in response to stimulation, to more complex input-output measures such as the transfer function[6–9]. The latter is related to the mean stimulus waveform that triggers an action potential: the so-called spike-triggered average or reverse correlation[10], which is also widely used[11,12]. Most recently, information-theoretic techniques have gained acceptance as efficient methods for quantifying the amount of information about a stimulus that is carried in a neuron's spike train[1,2]. These techniques quantify the amount of information available for decoding by postsynaptic cells[1] and have the advantage of incorporating the effects of neural dynamics, including bursting[13], oscillations[14] and chaos[15].

Here we show that correlations in a single neuron's spike train are important in shaping its information transmission properties. We examined patterns of neural activity in a well-studied model system, weakly electric fish. These fish reliably detect weak low-frequency signals generated by prey organisms[16]. Conventional encoding measures, such as transfer function, indicate that receptor afferent tuning is poorly matched to these important signals. However, information-theoretic measures of tuning indicate that the afferents respond well to

prey-like stimuli. We provide the first experimental proof that spike train correlations lead to increased information about low-frequency signals by reducing low-frequency noise, as predicted by previous modeling studies[17,18]. By simultaneously recording from pairs of receptor afferents, we show that this noise reduction is preserved across the afferent population. Finally, by recording from postsynaptic cells, we verify that the increased information about low-frequency stimuli is actually decoded and made available to cells at higher levels of the processing hierarchy.

RESULTS

Conventional tuning predicts poor responses to prey

We recorded activity from a class of sensory neurons, electroreceptor afferents, in the gymnotiform weakly electric fish *A. leptorhynchus*. These animals produce a continuous electric organ discharge (EOD) that functions as a carrier signal. Behaviorally relevant stimuli include amplitude modulations of this carrier ranging from a few hertz to in excess of 100 Hz. Different stimulus categories can be associated with unique spatiotemporal characteristics[16,19,20]. In addition, specific CNS subdivisions (spatiotopic maps) are clearly linked to processing of information relevant to specific behavioral contexts[20,21]. This study focuses on the animal's ability to detect weak low-frequency (< 30 Hz) amplitude modulations of the EOD caused by prey organisms[16]. This, as well as previous work[9,22] using conventional measures of receptor afferent tuning, all indicate a substantial mismatch between the frequency content of prey stimuli and receptor afferent tuning: receptor afferents are described as being most sensitive to frequencies far higher than those typically produced by prey (**Fig. 1a,b**). We characterized their tuning both in terms of a commonly used[23] phase-locking

[1]Department of Zoology, University of Oklahoma, 730 Van Vleet Oval, Norman, Oklahoma 73019, USA. [2]Department of Cellular and Molecular Medicine, University of Ottawa, 451 Smyth Road, Ottawa, Ontario K1H 8M5, Canada. Correspondence should be addressed to M.J.C. (mauricejchacron@yahoo.ca).
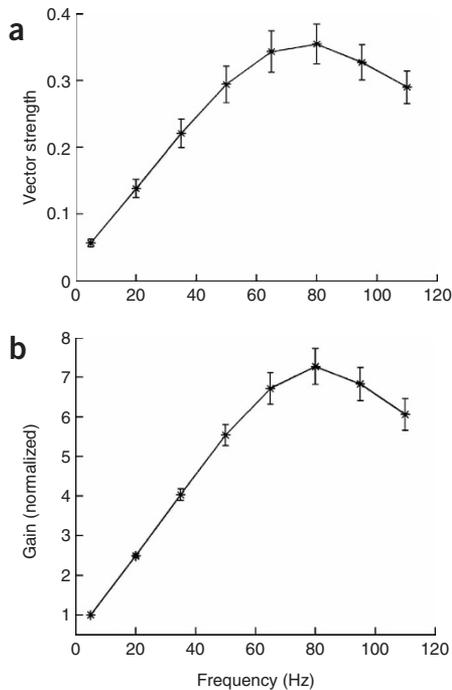
Figure 1 Responses of receptor afferents to sinusoidal amplitude modulations of the EOD. (**a**) Vector strength tuning curve averaged across 41 receptor afferents. Error bars indicate ± 1 s.e.m. The vector strength shows a maximum at a frequency of 84.24 ± 3.14 Hz. (**b**) Gain tuning curve averaged across the same population. Error bars indicate ± 1 s.e.m. Gain shows a maximum at a frequency of 85.21 ± 3.36 Hz, similar to that of the vector strength curve ($P = 0.42$, pairwise t-test, $n = 41$). The gain was normalized by its value at 1 Hz.

measure, vector strength (**Fig. 1a**; see Methods), as well as the gain curve from transfer function analysis (**Fig. 1b**). Both measures showed extremely poor responsiveness to low-frequency stimuli. These results seemingly contradict the frequent observation that sensory system tuning optimizes sensitivity to behaviorally important stimuli[1,24] and raise the question of how these animals can efficiently capture prey given this apparent tuning mismatch.

Information tuning predicts good responses to prey

One can also use information theory to estimate neural tuning[1]. We determined information tuning curves using band-limited random amplitude modulations (RAMs), and we quantified responses as the stimulus–spike train coherence, a measure related to the output signal-to-noise ratio[1]. Coherence measures the fraction of the stimulus that can be decoded by linear means (see Methods). Conventional tuning curves can also be obtained from transfer function analysis of responses to RAM stimuli; these predicted poor responses to low-frequency stimuli similar to those seen with sinusoidal stimuli (**Fig. 2**). However, information tuning curves showed a broadband response (**Fig. 2**) with a peak well-matched to the peak frequency (25 Hz) produced by prey, as estimated from analysis of actual prey capture behavior[16].

Negative correlations reduce low-frequency noise

We now provide an explanation of this large difference between tuning curves determined by coherence versus transfer function analysis. Although both took into account the input-output relationship, only coherence was sensitive to the intrinsic dynamics of the system, because the spike train power spectrum was used in its calculation (see Methods). Electroreceptor afferent spike trains showed patterning, as their interspike intervals (ISIs) were not randomly distributed. Successive interspike intervals were, in fact, negatively correlated (**Fig. 3a**, inset). Modeling studies have shown that these negative ISI correlations act to regularize the spike train[17,18]. As predicted, this regularization reduced the low-frequency power of electroreceptor afferent spike trains as shown by the power spectrum of their spontaneous activity (**Fig. 3a**). This reduction in low-frequency power is equivalent to reducing

low-frequency noise. This noise shaping increases the potential for information transfer at low frequencies[18].

In order to verify the role of these ISI correlations in shaping the receptor afferent power spectrum, we randomly shuffled the ISI sequence (see Methods). This removes ISI correlations (**Fig. 3a**, inset) and increases low-frequency power (**Fig. 3a**). This confirms that removal of electroreceptor afferent intrinsic ISI correlations leads to higher power at low frequencies, thereby increasing the effective low-frequency noise level. We compared information tuning curves of normal responses to RAM stimuli (**Fig. 3b**) with tuning curves from data with ISIs randomly shuffled (**Fig. 3b**) to determine the consequences of this increased noise level for information transfer. Removal of ISI correlations greatly attenuated the low-frequency coherence, as expected, given that ISI shuffling increases low-frequency noise. In addition, the peak of the information tuning curve was shifted to higher frequencies (~ 60 Hz), closer to the peak frequencies of conventional tuning curves. Thus, electroreceptor afferent ISI correlations underlie the differences in estimates of frequency tuning that appear when the analysis is based on coherence rather than transfer function.

The noise reduction persists at the population level

This improved information about low-frequency stimuli is transmitted to higher order neurons, pyramidal cells, which receive the summed input from a population of receptor afferents. Pyramidal cells must decode this information if it is to be of use to the animal. Thus, it was important to verify that the reduction in low-frequency power seen in a single afferent's baseline activity was preserved when multiple activities are summed. Under baseline activity, this summed input would contain
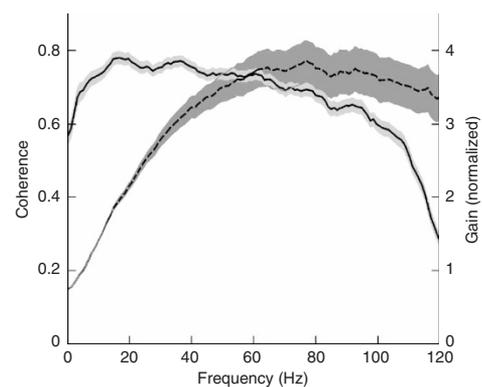
Figure 2 Responses of receptor afferents to random amplitude modulations of the EOD. Throughout, we used band-limited (0–120 Hz) white noise as the modulation signal. The average coherence curve, $C(f)$ (solid line), is plotted with the average gain curve, $G(f)$ (dashed line), for comparison. The gain curve shows a sharp maximum at 76.00 ± 6.43 Hz, a frequency that is not statistically different from that obtained with sinusoidal stimuli ($P = 0.49$, pairwise t-test, $n = 17$). The coherence curve is more broadband and peaks at a lower frequency (23.64 ± 2.22 Hz) than the gain curve ($P < 10^{-3}$, pairwise t-test, $n = 41$). The gain was normalized by its value at 1 Hz. Gray bands indicate ± 1 s.e.m.

Figure 3 Receptor afferent spike train characteristics. (**a**) Average ($n = 41$) power spectrum of receptor afferent baseline (that is, no EOD modulation) activity (solid line). The spectrum decays to a very low value at zero frequency and slowly increases and peaks at a frequency related to the spontaneous firing frequency of the afferent. The average power spectrum of shuffled spike trains (dashed line; see Methods) shows higher power at frequencies below 80 Hz. The inset shows the population-averaged ISI serial correlation coefficients ρ_j as a function of lag j (see Methods). A negative correlation coefficient is seen at lag 1 for the baseline spike train (solid line), whereas the shuffled spike train (dashed line) has $\rho_j = 0$ for $j > 0$. (**b**) Population-averaged coherence curve for receptor afferent responses to 0–120 Hz RAM stimuli (solid line). The predicted coherence curve (dashed line) based on the shuffled spike train is also shown (see Methods) and peaks at 59.34 ± 2.72 Hz, significantly higher than the peak of the unshuffled coherence ($P < 10^{-3}$, pairwise t-test, $n = 41$). Gray bands indicate ± 1 s.e.m.

low power at low frequencies if its power spectrum were simply given by the sum of individual receptor afferents' power spectra (**Fig. 3a**). However, correlated activity among receptor afferents could preclude this outcome (see Methods). Therefore, the data presented thus far does not prove that the summed input would also contain low power at low frequencies, as we could not detect correlated activity among receptor afferents recorded individually. To test for correlated activity, we performed simultaneous recordings from pairs of receptor afferents under both baseline and stimulated conditions. As expected, there was substantial correlation at frequencies associated with the fish's EOD, as it is a common input to both afferents (**Fig. 4a**). However, we did not observe this correlation at other frequencies, particularly in the frequency range of prey-like stimuli (**Fig. 4a**, inset). We verified this by randomly shuffling each afferent's ISI sequence, thereby removing all correlations at frequencies associated with the EOD (**Fig. 4a**). More notably, however, shuffling did not alter the cross-spectrum over the frequency range of the stimuli used (**Fig. 4a**, inset), verifying that the original spike trains were uncorrelated over the range of frequencies associated with prey-like stimuli. Cross-spectra based on normal and shuffled ISI sequences were integrated over 0–120 Hz and compared for
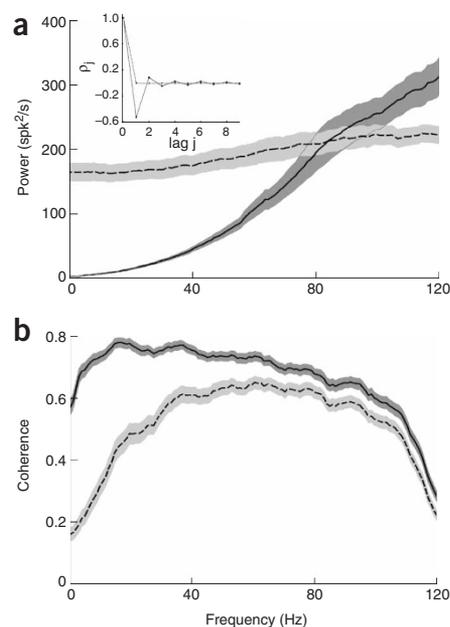
each receptor afferent pair. Their differences were not statistically significantly different from zero ($P = 0.55$, pairwise t-test, $n = 10$). Thus, no correlated activity in the 0–120 Hz frequency range was present in the original data. As in the case of single receptor afferents, the summed input from pairs of receptor afferents showed low power at low frequencies (**Fig. 4b**), and shuffling the ISIs greatly increased low-frequency power (**Fig. 4b**).

To verify that the reduced low-frequency power of pairs of afferents translated into increased information about low-frequency stimuli, we applied the same RAM stimulus to each pair. The average coherence curves (**Fig. 5a**) from the summed activity of pairs and from single afferents (**Fig. 2**) had similar shapes, and both indicated greatly improved information transfer at low frequencies as compared with more conventional tuning measures derived from transfer function analysis (**Fig. 5a**). Thus, the same differences between the coherence and conventional tuning measures are seen for individual receptor afferents as well as at the afferent population level. Given these different estimates of receptor afferent population tuning, it was important to determine which best described the message conveyed to the CNS, or in other words, which measure of tuning best predicted the output of the postsynaptic neurons that decode electroreceptor afferent input.

The brain decodes information from receptor afferents
In order to resolve this issue, we recorded the response of the postsynaptic targets of receptor afferents, pyramidal cells, to identical RAM stimuli. Conventional pyramidal cell tuning curves as well as
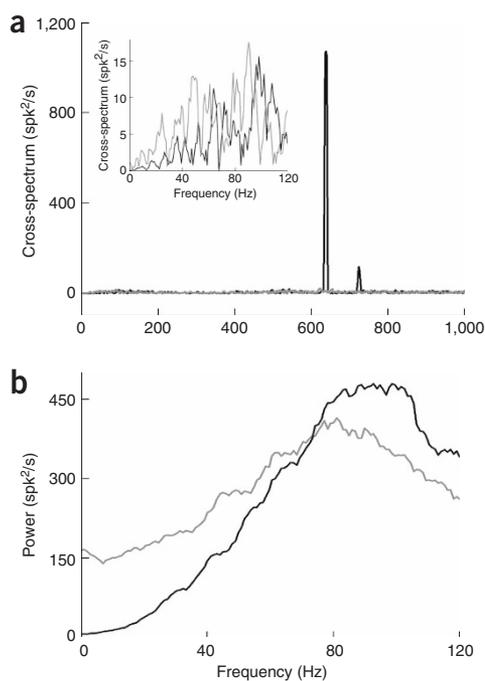
Figure 4 Characteristics of the afferent population. (**a**) An example cross-spectrum (absolute value) between a pair of receptor afferents that were recorded from simultaneously. The raw data (black line) shows that there is no substantial correlation except at frequencies associated with the fish's own EOD (≈ 700 Hz). The cross-spectrum between the two resulting spike trains is also shown (gray line). The inset shows the two curves over the 0–120 Hz frequency range, and no significant difference is seen over that range. (**b**) Power spectrum of the summed activity for that pair (black line) and for the summed activity of the shuffled spike trains (gray line). Low power at low frequencies is seen in the raw data, and ISI shuffling increases this low-frequency power.
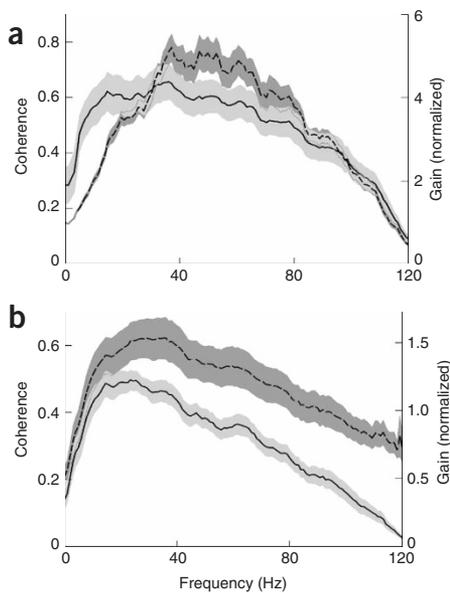
Figure 5 Tuning properties of higher order neurons. (**a**) Population-averaged coherence (solid line) and gain (dashed line) curves for the ten pairs of afferents from which recordings were made. The gain was normalized by its value at 1 Hz. The coherence and gain curves peak at different frequencies that averaged 28.32 ± 11.89 Hz and 46.19 ± 12.51 Hz for the coherence and gain curves, respectively ($P = 0.003$, pairwise t-test, $n = 10$). (**b**) Response of higher-order neurons (ELL pyramidal cells) to random stimuli. Average ($n = 10$) gain (solid line) and coherence (dashed line) curves show maxima at 29.8 ± 2.77 Hz and 23.5 ± 2.69 Hz, respectively ($P = 0.09$, pairwise t-test, $n = 10$). Gray bands indicate ± 1 s.e.m.

information tuning curves (**Fig. 5b**) both showed maxima between 20 and 30 Hz. Neither the maxima of pyramidal cell tuning curves determined by coherence or transfer function analysis were significantly different from that of receptor afferent information tuning curves (**Fig. 2**), which averaged about 24 Hz ($P = 0.98$ and 0.36, respectively, t-tests, 51 degrees of freedom). However, both estimates of pyramidal cell tuning were significantly less than receptor afferent tuning determined with either vector strength or transfer function analysis. For example, the peak frequency of the gain tuning curve for pyramidal cells was significantly different from the peak frequency obtained from the gain curve of receptor afferents ($P < 10^{-3}$, t-test, 51 degrees of freedom). Thus, pyramidal cell responses reflected receptor afferent information tuning more closely than it reflected receptor afferent tuning determined with more classical techniques. Furthermore, the improved receptor afferent low-frequency responsiveness shown by information tuning resulted in a wider receptor afferent bandwidth, facilitating the transmission of information relevant to prey detection and capture as well as other behaviorally relevant stimuli.

DISCUSSION

We have shown that although two different classical measures of tuning agree well with one another, there are significant differences between these and information tuning curves for receptor afferents. This difference is due to strong ISI correlations seen in receptor afferent spike trains that lead to a shaping of the baseline power spectrum (noise shaping). As receptor afferents are not correlated over the frequency range of behaviorally relevant stimuli, the summed input from a population of receptor afferents will also show similar shaping of its

baseline power spectrum. Noise shaping is commonly observed in engineering devices[25], and theoretical studies have postulated as to its putative role for it in brain function[18,26–28]. This is the first experimental demonstration of such effects *in vivo*: noise shaping improves the responses of neurons to naturalistic stimuli by reducing noise within a specific frequency range.

Modeling studies have shown that calcium-activated potassium currents can lead to negative ISI correlations[29,30]. These currents are present in electroreceptors[31]; thus, they could presumably contribute to the negative ISI correlations seen here. These correlations are present in other systems as well at both the peripheral and the cortical level[32–34], and calcium-activated potassium currents are also seen in a variety of neurons[35]. Thus, the influence of negative ISI correlations on information transfer could be a general feature of sensory processing. Furthermore, numerous other types of dynamics such as bursting[13], oscillations[14] and chaos[15] exist, raising the possibility of a rich repertoire of dynamic effects on information transfer. However, not all neural variables will have an influence on information transmission: a previous study has found that neural refractoriness increased the precision of spike timing yet had no significant effects on information tuning[36].

When the goal is to understand the relationship between an animal's nervous system function and its behavior, it is important to consider the information that is decoded by the postsynaptic cell. Recordings from the pyramidal cells showed that both their classical and information tuning were most similar to receptor afferent information tuning. The lack of qualitative differences between classical and information tuning for the subset of pyramidal cells studied reflects their lack of significant intrinsic spike train dynamics[37]. Although the importance of using information-theoretic measures over more conventional measures has been advocated before[1,38], only a few studies have actually compared the two, and these found little or no qualitative difference between them[39]. This is the first instance in which major qualitative differences between the transfer and coherence functions have been observed and attributed to negative ISI correlations.

The neural code must capture information critical to an animal's survival. Formal properties of a code include a transformation or encoding process as well as an interpretation or decoding process. Encoding capabilities are typically estimated via transfer functions or reverse correlation techniques[12,39] that are, in fact, equivalent for white noise stimuli[40]. These techniques are commonly used to estimate the shape of both visual spatiotemporal[41] and auditory spectrotemporal[12] receptive fields. The decoding abilities of postsynaptic targets can be estimated through the information tuning curves presented here[1], and we have shown that spike train dynamics can have profound effects on the information that can be recovered by a postsynaptic cell. Therefore, as previously suggested[1], decoding measures that include the effects of neural dynamics might be more appropriate measures of neural tuning. How these will affect estimates of receptive field organization is presently unknown. Our analysis shows that using decoding measures based on information theory may lead to improved understanding of the ways sensory neurons process behaviorally relevant stimuli.

Although transfer function analysis remains an important tool to characterize the input-output properties of systems in many fields, many biological and non-biological systems are capable of rich dynamics[42]. These dynamics can potentially alter their responses to input as seen from the point of view of the decoder.

METHODS

Stimulation and recording. We used the weakly electric fish species *A. leptorhynchus* in this study. The experimental protocol has been previously described in detail[43]. The stimuli consisted of sinusoidal and band-limited

(0–120 Hz) random amplitude modulations of an animal's own EOD presented with global geometry (note that receptor afferent responses are insensitive to the spatial extent of the stimulus[43]). Extracellular single-unit recordings from pyramidal cells in the centrolateral and lateral segments were made with metal-filled microelectrodes. Pyramidal cells in these segments have been shown to respond to medium and high-frequency stimuli, respectively[21]. Intracellular recordings from receptor afferents were made with 40–100 MΩ, KCl-filled micropipettes. Only pyramidal cells with a firing frequency greater than 30 Hz (deep basilar pyramidal cells[37]) were included in the data sample, as their responses are directly driven by receptor afferent input and their baseline spike trains lack ISI correlations[43]. Responses of these pyramidal cells simply decode the afferent input with minimal complications owing to intrinsic pyramidal cell dynamics or circuitry. Other pyramidal cells are more selective in their responses and do respond exclusively to low-frequency stimuli when the stimulus' spatial extent is prey-like[44]. Furthermore, these same cells shift their frequency preference to a higher range when the stimulus' spatial characteristics are communication-like[44]. Standard electro-physiological methods were used; data were acquired with Cambridge Electronic Design (CED) 1401 plus hardware and SpikeII software. All surgical procedures were in accordance with the University of Oklahoma animal care and use guidelines.

Data analysis. All data analysis was performed using Matlab (Mathworks). Baseline activity was characterized using the interspike interval distribution as well as the ISI serial correlation coefficients defined as $\rho_j = \; < I_i I_{i+j} - <I_i>^2 > \; / \; < I_i I_i - <I_i>^2 >$. Here, $< \ldots >$ denotes averaging over index i, and j is the lag. By definition, $\rho_0 = 1$. When the ISIs are independent and identically distributed, we have a renewal process, and $\rho_j = 0$ for $j > 0$. However, if $\rho_j \neq 0$ for any $j > 0$, the process is non-renewal. We also computed the spike train power spectrum $P_0(f)$ of baseline activity. In order to eliminate ISI correlations, we randomly shuffled the ISI sequence. We then computed the spike train power spectrum $P_{0,\text{shuffled}}(f)$ of the resulting spike train.

Spike trains during sinusoidal amplitude modulation (SAM) stimulation were accumulated as phase histograms. Vector strength, which ranges between 0 (no phase locking) and 1 (perfect phase locking), was used to measure responses in terms of synchronization to the SAM stimulus. In addition, system gain $G(f) = |P_{sx}(f)|/P_{ss}(f)$ was used to quantify the system's amplification as a function of stimulus frequency f. Responses to RAM stimulation were also analyzed by computing the system gain as well as the coherence function $C(f) = |P_{sx}(f)|^2/(P_{ss}(f) \, P_{xx}(f))$, where $P_{ss}(f)$ and $P_{xx}(f)$ are the power spectra of the stimulus and spike train under driven activity, respectively. $P_{sx}(f)$ is the cross-spectrum between the stimulus and the spike train. The coherence $C(f)$ ranges between 0 and 1 and represents the fraction of frequency component f that can be decoded by linear means[2,39]. Population-averaged values are given throughout the paper as mean ± 1 s.e.m.

The degree to which two spike trains were correlated was quantified by computing the absolute value of the cross-spectrum between the pair. The cross-spectrum is the inverse Fourier transform of the cross-correlation function. Given two spike trains W and Y, the power spectrum of the summed input $Z = W + Y$ is then given by the formula $P_{zz} = P_{ww} + P_{yy} + 2 \, \text{Re}(P_{wy})$. Here, P_{ww} and P_{yy} are the power spectra of W and Y, respectively. P_{wy} is the cross-spectrum between W and Y, whereas $\text{Re}(P_{wy})$ denotes the real part of P_{wy}. Thus, correlated activity would preclude the power spectrum of the summed input simply being the sum of the power spectra of each individual input.

Random shuffling of the ISI sequence obtained under driven conditions not only eliminates any intrinsic ISI correlations but also eliminates correlations owing to the stimulus. In order to circumvent this problem, we used linear response theory[45] to approximate the shuffled spike train power spectrum obtained under driven activity by $P_{xx,\text{shuffled}}(f) \approx P_{0,\text{shuffled}} + G(f)^2 P_{ss}(f)$. This equation has been used successfully before with neuron models,[18] and it provides a good approximation of the driven power spectrum $P_{xx}(f)$ in the control case (data not shown).

1. Rieke, F., Warland, D., de Ruyter van Steveninck, R.R. & Bialek, W. *Spikes: Exploring the Neural Code* (MIT, Cambridge, Massachusetts, USA, 1996).
2. Borst, A. & Theunissen, F. Information theory and neural coding. *Nat. Neurosci.* **2**, 947–957 (1999).
3. Holden, A.V. Signal processing: neural coding by correlation? *Nature* **428**, 382 (2004).
4. Hubel, D.H. & Wiesel, T.N. Receptive fields and functional architecture of the monkey striate cortex. *J. Physiol. (Lond.)* **195**, 215–243 (1968).
5. Barlow, H.B. & Levick, W.R. Changes in the maintained discharge with adaptation level in the cat retina. *J. Physiol. (Lond.)* **202**, 699–718 (1969).
6. Cook, E.P. & Maunsell, J.H.R. Attentional modulation of motion integration of individual neurons in the middle temporal visual area. *J. Neurosci.* **24**, 7964–7977 (2004).
7. Eggermont, J.J. Temporal modulation transfer functions for single neurons in the auditory midbrain of the leopard frog. Intensity and carrier-frequency dependence. *Hear. Res.* **43**, 181–198 (1990).
8. Goldberg, J.M. & Fernandez, C. Physiology of peripheral neurons innervating semicircular canals of the squirrel monkey. II. Response to sinusoidal stimulation and dynamics of peripheral vestibular system. *J. Neurophysiol.* **34**, 661–675 (1971).
9. Nelson, M.E., Xu, Z. & Payne, J.R. Characterization and modeling of P-type electrosensory afferent responses to amplitude modulations in a wave-type electric fish. *J. Comp. Physiol. [A]* **181**, 532–544 (1997).
10. de Boer, E. & Kuyper, P. Triggered correlation. *IEEE Trans. Biomed. Eng.* **15**, 159–179 (1968).
11. Dayan, P. & Abbott, L.F. *Theoretical Neuroscience: Computational and Mathematical Modeling of Neural Systems* (eds. Sejnowski, T.J. & Poggio, T.) 45–85 (MIT, Cambridge, Massachusetts, USA, 2001).
12. Theunissen, F.E., Woolley, S.M., Hsu, A. & Fremouw, T. Methods for the analysis of auditory processing in the brain. *Ann. NY Acad. Sci.* **1016**, 187–207 (2004).
13. Wang, X.J. & Rinzel, J. in *The Handbook of Brain Theory and Neural Networks* (ed. Arbib, M.A.) 686–691 (MIT Press, Cambridge, Massachusetts, USA, 1995).
14. Gray, C. & Singer, W. Stimulus-specific neuronal oscillations in orientation columns of cat visual cortex. *Proc. Natl. Acad. Sci. USA* **86**, 1698–1702 (1989).
15. Korn, H. & Faure, P. Is there chaos in the brain? II. Experimental evidence and related models. *C.R. Biol.* **326**, 787–840 (2003).
16. Nelson, M.E. & MacIver, M.A. Prey capture in the weakly electric fish Apteronotus leptorhynchus: sensory acquisition strategies and electrosensory consequences. *J. Exp. Biol.* **202**, 1195–1203 (1999).
17. Chacron, M.J., Longtin, A. & Maler, L. Negative interspike interval correlations increase the neuronal capacity for encoding time-varying stimuli. *J. Neurosci.* **21**, 5328–5343 (2001).
18. Chacron, M.J., Lindner, B. & Longtin, A. Noise shaping by interval correlations increases information transfer. *Phys. Rev. Lett.* **92**, 080601 (2004).
19. Zupanc, G.K.H. & Maler, L. Evoked chirping in the weakly electric fish *Apteronotus leptorhynchus*: a quantitative biophysical analysis. *Can. J. Zool.* **71**, 2301–2310 (1993).
20. Metzner, W. & Juranek, J. A sensory brain map for each behavior? *Proc. Natl. Acad. Sci. USA* **94**, 14798–14803 (1997).
21. Shumway, C. Multiple electrosensory maps in the medulla of weakly electric Gymnotiform fish. I. Physiological differences. *J. Neurosci.* **9**, 4388–4399 (1989).
22. Bastian, J. Electrolocation I. How the electroreceptors of Apteronotus albifrons code for moving objects and other electrical stimuli. *J. Comp. Physiol. [A]* **144**, 465–479 (1981).
23. Carr, C.E. & Konishi, M. A circuit for detection of interaural time differences in the brain stem of the barn owl. *J. Neurosci.* **10**, 3227–3246 (1990).
24. Rieke, F., Bodnar, D.A. & Bialek, W. Naturalistic stimuli increase the rate and efficiency of information transmission by primary auditory afferents. *Proc. R. Soc. Lond. B* **262**, 259–265 (1995).
25. Norsworthy, S.R., Schreier, R. & Temes, G.C. (eds.) *Delta-Sigma Data Converters* (IEEE, Piscataway, New Jersey, USA, 1997).
26. Shin, J. Novel neural circuits based on stochastic pulse coding noise feedback pulse coding. *Int. J. Electron.* **74**, 359–368 (1993).
27. Shin, J. Adaptation in spiking neurons based on the noise shaping neural coding hypothesis. *Neural Netw.* **14**, 907–919 (2001).
28. Mar, D.J., Chow, C.C., Gerstner, W., Adams, R.W. & Collins, J.J. Noise shaping in populations of coupled model neurons. *Proc. Natl. Acad. Sci. USA* **96**, 10450–10455 (1999).
29. Wang, X.J. Calcium coding and adaptive temporal computation in cortical pyramidal neurons. *J. Neurophysiol.* **79**, 1549–1566 (1998).
30. Liu, Y.H. & Wang, X.J. Spike frequency adaptation of a generalized leaky integrate-and-fire neuron. *J. Comput. Neurosci.* **10**, 25–45 (2001).
31. Bennett, M.V.L. & Obara, S. in *Electroreception* (eds. Bullock, T. H. & Heiligenberg, W.) 157–181 (Wiley, New York, 1986).
32. Lowen, S.B. & Teich, M.C. Auditory-nerve action potentials form a nonrenewal point process over short as well as long time scales. *J. Acoust. Soc. Am.* **92**, 803–806 (1992).
33. Klemm, W.R. & Sherry, C.J. Serial ordering in spike trains: what's it 'trying to tell us'? *Int. J. Neurosci.* **14**, 15–33 (1981).

34. Lebedev, M.A. & Nelson, R.J. High-frequency vibratory sensitive neurons in monkey primate somatosensory cortex: entrained and nonentrained responses to vibration during the performance of vibratory-cued hand movements. *Exp. Brain Res.* **111**, 313–325 (1996).

35. Stocker, M. Ca^{2+}-activated K$^+$ channels: molecular determinants and function of the SK family. *Nat. Rev. Neurosci.* **5**, 758–770 (2004).

36. Berry, M.J., II & Meister, M. Refractoriness and neural precision. *J. Neurosci.* **18**, 2200–2211 (1998).

37. Bastian, J. & Nguyenkim, J. Dendritic modulation of burst-like firing in sensory neurons. *J. Neurophysiol.* **85**, 10–22 (2001).

38. Warland, D.K., Reinagel, P. & Meister, M. Decoding visual information from a population of retinal ganglion cells. *J. Neurophysiol.* **78**, 2336–2350 (1997).

39. Theunissen, F., Roddey, J.C., Stufflebeam, S., Clague, H. & Miller, J.P. Information theoretic analysis of dynamical encoding by four identified interneurons in the cricket cercal system. *J. Neurophysiol.* **75**, 1345–1364 (1996).

40. Gabbiani, F. & Koch, C. in *Methods in Neuronal Modeling: From Ions to Networks* (eds. Koch, C. & Segev, I.) 313–360 (MIT Press, Cambridge, Massachusetts, USA, 1998).

41. Jones, J. & Palmer, L. The two-dimensional spatial structure of simple receptive fields in cat striate cortex. *J. Neurophysiol.* **58**, 1187–1211 (1987).

42. Strogatz, S.H. *Nonlinear Dynamics and Chaos: With Applications to Physics, Biology, Chemistry, and Engineering* (Perseus Books, Reading, Massachusetts, USA, 1994).

43. Bastian, J., Chacron, M.J. & Maler, L. Receptive field organization determines pyramidal cell stimulus-encoding capability and spatial stimulus selectivity. *J. Neurosci.* **22**, 4577–4590 (2002).

44. Chacron, M.J., Doiron, B., Maler, L., Longtin, A. & Bastian, J. Non-classical receptive field mediates switch in a sensory neuron's frequency tuning. *Nature* **423**, 77–81 (2003).

45. Risken, H. *The Fokker-Planck Equation* (Springer, Berlin, 1996).